SAND2023-06741C

Data-Driven Model Predictive Control for Fast-Frequency Support

Astha Rai
Electrical and Computer Engineering
University of Maine
Orono, Maine, USA
astha.rai@maine.edu

Niranjan Bhujel
Electrical and Computer Engineering
University of Maine
Orono, Maine, USA
niranjan.bhujel@maine.edu

Ujjwol Tamrakar
Energy Storage Tech and Systems
Sandia National Laboratories
Albuquerque, New Mexico, USA
utamrak@sandia.gov

Donald Hummels
Electrical and Computer Engineering
University of Maine
Orono, Maine, USA
donald.hummels@maine.edu

Reinaldo Tonkoski
Electrical and Computer Engineering
University of Maine
Orono, Maine, USA
reinaldo.tonkoski@maine.edu

***Abstract*—Low-inertia microgrids experience significant frequency deviations compared to bulk-power systems. In such microgrids, energy storage systems (ESSs) can be a viable option to provide fast-frequency support to keep frequency variations within allowable bounds. A model predictive control (MPC)-based strategy is one of the efficient control strategies to enable fast-frequency support through ESSs. MPC provides the capability to explicitly incorporate physical constraints of the microgrid and the ESS into the control formulation while allowing significant operational flexibility. MPC allows near-optimal control by optimizing the system over a rolling horizon based on a *predictive model* of the system. However, the effectiveness of MPC relies on the accuracy of this predictive model. This paper proposes a data-driven system identification (SI) based approach to obtain an accurate yet computationally tractable predictive model for frequency support in microgrids. The proposed data-driven MPC is compared with the conventional MPC that utilizes a simplified transfer-function-based predictive model of the system. Results show that the data-driven MPC offers a better quality of service in terms of lower frequency deviations and rate-of-change of frequency (ROCOF).**

***Index Terms*—Model predictive control, energy storage system, system identification, fast-frequency support.**

I. Introduction

A microgrid is composed of distributed energy resources (DERs) and loads, with PV and wind integrated via power-electronic inverters. Utilization of power-electronic inverters in microgrids reduces the inertia of the system compared to traditional rotational generation-based systems. As a result, frequency variations arise from imbalances between load and generation, which are more extreme in low-inertia systems. Failure to restore frequency to its nominal value can lead to power outages. One of the possible solutions is to provide frequency support during transients using an energy storage system (ESS). The ESS can discharge or charge when the grid experiences low or high frequency based on an appropriate control mechanism and provide frequency support. This paper proposes a model predictive control (MPC) to provide such control actions through an ESS.

MPC provides a flexible framework to support the power system voltage and frequency in microgrids [1], [2]. MPC provides near-optimal control actions using a *predictive model* of the system. However, finding a suitable predictive model that accurately represents the system dynamics while being computationally tractable is challenging. The problem is exacerbated when the faster system dynamics are being modeled and the MPC needs to be solved in real-time with control time steps in ms or μs ranges. Finding the right balance between accuracy and computational feasibility is critical to ensure the effectiveness of MPC. In [2], the frequency dynamics of a microgrid system is modeled using a "swing equation" and the turbine-governor dynamics equation. However, this model becomes insufficient as the system expands and its dynamics change over time. Data-driven system identification techniques, which do not rely on prior assumptions of power system dynamics offer an alternative approach to modeling the system. However, previous research in this area has primarily focused on load frequency control [3], [4]. In [5], data-driven grid-supporting control for islanded microgrids using an H_∞ filter is presented; nevertheless, the H_∞ filter lacks the flexibility to adjust parameters as effectively as MPC. The authors in [6] proposed an online frequency characteristic estimator and an online optimization controller designed based on MPC. However, the authors have only considered

This work is supported by the US Department of Energy, Office of Electricity, Energy Storage Program.

frequency deviation as a controllable state. In contrast, our research goes beyond this work by incorporating the rate-of-change of frequency (ROCOF) as an additional controllable parameter. Leveraging the inherent flexibility of MPC, our methodology allows for prioritization and customization of the states and control signals according to specific requirements and objectives as mentioned in [2].

In this paper, we propose a data-driven MPC for fast-frequency support. The main contributions of this paper are as follows:

1) Developed a system identification based approach to obtain a data-driven model of microgrid using an appropriate excitation signal.
2) Presented specific requirements for the design of the aforementioned excitation signal to extract the frequency dynamics of microgrid systems.
3) Developed a data-driven MPC-based approach for providing fast-frequency support utilizing ESS with better quality of service in terms of frequency and ROCOF minimization.

The paper is organized as follows: Section II describes the SI methodology in which the chirp signal design and parameters are explained. MPC-based frequency support approach along with the base case and formulation is presented in Section III. Sections IV and V show the model validation and results respectively. Finally, Section VI concludes the paper.

II. System Identification Methodology

System identification (SI) refers to building a mathematical model of a dynamic system based on the observed data from the system [7]. The process of SI of a dynamic system is shown in Fig. 1. The system is excited with an input signal and the output data is observed. Then, the data are used to identify the system through a transfer function (TF) representation.

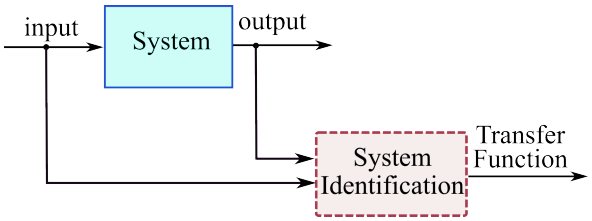

Fig. 1: System identification (SI) basic concept – using the input-output data to estimate the transfer function of a system.

A. Design of Excitation Signal

The design of the input signal (excitation signal) of the system plays a significant role in exciting the dynamics of interest and ensuring that the desired information of the system behavior can be extracted. The excitation signal should be able to provide an accurate estimate of the system while maintaining safe operation of the power system. Desired characteristics for an excitation signal design include – a high signal-to-noise ratio (SNR), a longer-duration signal with excitation in frequencies of interest for the desired application, and a sampling rate high enough to represent all frequencies of interest [8]. Considering the aforementioned factors, in this work the system is excited using a chirp signal, which covers a wide frequency range. More specifically, a logarithmic square chirp signal is selected because square signals, with their rich harmonic content, can be useful for capturing the dynamic response of a system across a wider frequency range. In [9], different chirp signals were used to perturb a commercial off-the-shelf inverter. Among different signals, the logarithmic square chirp signal performed the best to extract the dynamics of the inverter.

The design parameters of a logarithmic chirp signal are the lower frequency f_l, the higher frequency f_h, the time to reach from f_l to f_h, T, and the amplitude A as illustrated in Fig. 2. Algorithm 1 shows the chirp signal design and calculates the frequency of interest of the system. First, to calculate f_l, the settling time of the system is obtained by exciting the system with a step signal. In our case, we have an input step signal of amplitude 0.05 p.u. with which we perturbed the microgrid system. The objective is to observe the system's output response and identify the settling time. The output (micorgrid's frequency) is observed using a phase-locked loop (PLL) which gives noisy measurements. The settling time of the system can be calculated measuring the time it takes for the system's output response curve to stabilize within a specified range (typically 2% or 5%) of the final steady-state value [10]. The settling time of the frequency response after applying the step input is 40s.

Next, the computed settling time of the frequency response curve is utilized to calculate the most significant time constant. According to the rule of thumb, the most significant time constant is approximately one-fifth of the settling time. This rule provides a rough estimation of the dominant time constant in the system based on the time it takes for the frequency response to stabilize. The reciprocal of the time constant gives the lower frequency f_l as 0.02Hz.

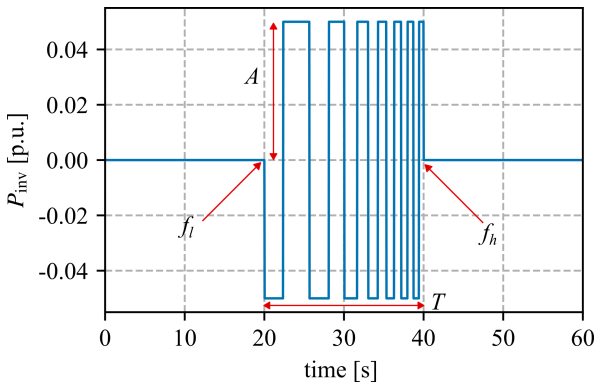

Fig. 2: Logarithmic Chirp Signal Parameters.

Next, the value of f_h needs to be calculated. Algorithm 1, calculates the value of f_h by using an iterative process and requires an initial guess. However, due to the limit in the bandwidth of PLL, the estimate of f_h can diverge instead of converging to a specific value. To address this issue, it is

Algorithm 1: Chirp Signal Design Algorithm

1. Excite the system using step signal
2. Calculate the f_{l} based on the settling time
3. Guess f_{h} and calculate T
4. Design excitation signal using $f_{\mathrm{l}}, f_{\mathrm{h}}$

for *Excitation signal* **do**
- Run the model
- Calculate the transfer function and eigenvalues
- Use the Eigenvalues to calculate new $f_{\mathrm{h,new}}$
- limit $f_{\mathrm{h,new}}$ in $f_{\max}$
- Design excitation signal with new $f_{\mathrm{h,new}}$

While $f_{\mathrm{h}} \neq f_{\mathrm{h,new}}$

necessary to impose an upper limit f_{max} on the estimate of f_h by considering the PLL's bandwidth. To determine f_{max}, a $3-\phi$ signal with a frequency of 60 Hz is applied to the PLL, and the input and output signals are tracked and recorded. Fig. 3 shows the bode plot of the PLL's response when the bandwidth of the PLL is varied from 0.01 Hz to 25 Hz. Ideally, the gain and phase of the bode plot must be 0 dB and 0° respectively for perfect tracking. As we increase the frequency, the gain and phase of the response starts to deviate from its ideal value. In this particular case, the frequency value at a gain of $20\log\left(\frac{1.05}{1}\right) = 0.41$ dB (5% deviation) is used which gives us 3.47Hz as the $f_{\max}$ value in Algorithm 1.

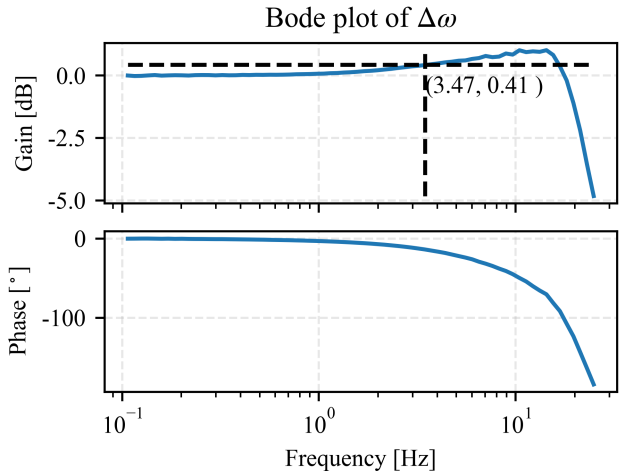

Fig. 3: Bode Plot of PLL.

For the initial guess of f_h any initial guess can be selected. In this case, we have chosen 2 Hz which is below f_{max}. Using this initial guess, f_h is calculated as 3 Hz. Then, T is calculated using the frequency range and the rate of the exponential increase of frequency [11] which is shown in (1) which results in 250s.

$$T = \frac{log_e(f_h/f_l)}{f_l}\left(N + \frac{\phi_0}{2\pi}\right) \tag{1}$$

where ϕ_0 is the initial phase and is 0, and $N = 1$

The parameters are summarized in Table I. The amplitude chosen is 0.05 p.u. (a low amplitude probing signal). The higher amplitude signal creates a higher perturbation signal which has higher SNR which makes the transfer function learning process easy. However, it might impact the power system frequency stability. The designed logarithmic chirp signal characterized by these parameters is shown in Fig. 4 (a). Fig. 4 (b) illustrates how the frequency of the signal changes over time.

TABLE I: Parameter of the square log chirp signal

Parameter	Value	Parameter	Value
f_l	0.02 Hz	T	250 s
f_h	3 Hz	A	0.05 p.u.

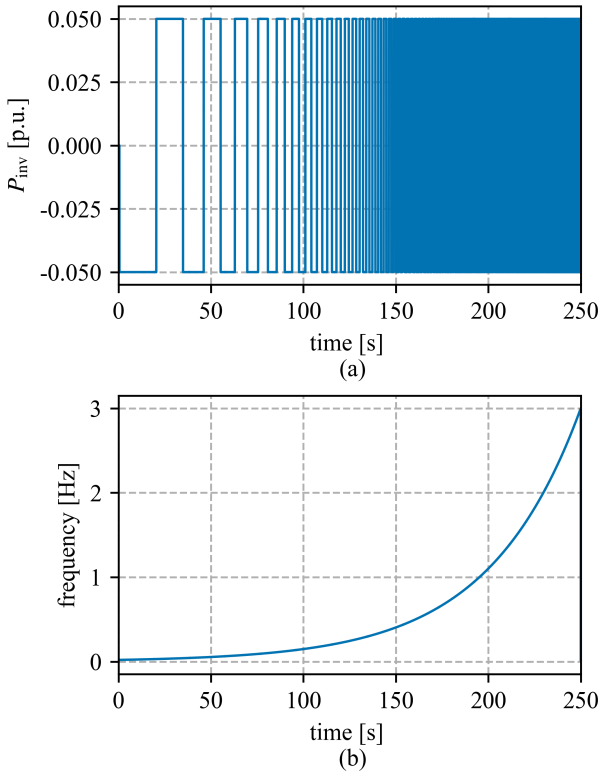

Fig. 4: (a) Logarithmic square chirp having $f_l = 0.02$ Hz and $f_h = 3$ Hz, $T = 250$s and $A = 0.05$[p.u.] (b) exponential increase of frequency with time. $f = 0.02$Hz at $t = 0$s and $f = 3$Hz at $t = 250$s.

III. Model Predictive Control and Kalman Filter for Frequency Support

The controller's primary goal is to quickly restore the frequency of a microgrid system following a frequency event to lower ROCOF and the frequency deviation. The MPC, fulfilling system constraints, provides a set of potential future control actions by minimizing the desired cost function for a given predictive model. Only the first control action of the series is applied to the system at a given timestep. MPC continues to solve the optimization problem at each sampling instant over a finite horizon. To facilitate MPC's operation, a dynamic state estimator is required to estimate the system states. In [12], various filters were compared for state and parameter estimation in power system frequency dynamics. The evaluation focused on the accuracy of state

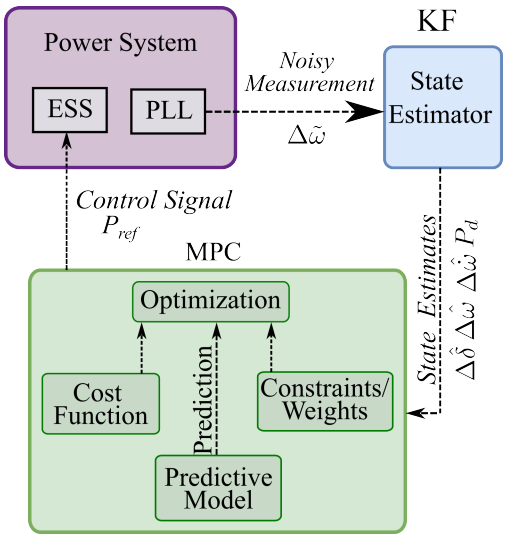

Fig. 5: Simulation setup for the fast-frequency support using KF-MPC approach

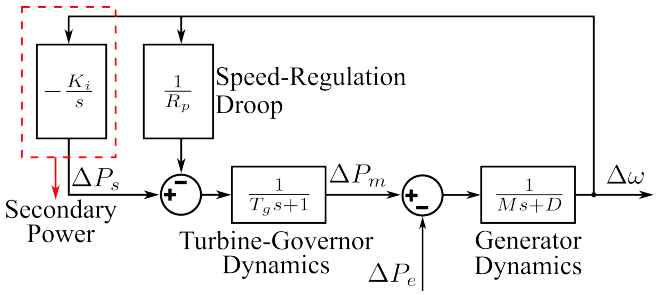

Fig. 6: Transfer function representation of an isolated microgrid [2]

and parameter estimation as well as computational costs. The results highlighted that a Kalman filter (KF) can be utilized for state estimation if the main objective is to estimate the states alone. Thus, a KF state estimator is employed in our approach to estimating the necessary states for MPC using frequency measurements. The details of the KF are in [12]. Fig. 5 provides an overview of the general MPC-KF-based approach, where the KF is responsible for state estimation, while MPC generates the control signal to be applied to the microgrid.

A. MPC Formulation

Let N be defined as the length of the time horizon and $\{0, 1, 2, ..., N-1\}$ be the set of discrete sample times in the forward time horizon, x_k are the states which will be computed using SI and y_k ($y_k = Cx_k$) be the discretized state equation, and Δu_k be the control input (ESS inverter power). The MPC is formulated from [2] as:

$$\min_{x,\ u} J = \sum_{k=0}^{N-1} (y_k^T Q y_k + \Delta u_k^T R \Delta u_k) + y_N^T Q y_N$$

subject to

$$x_{k+1} = F(x_k, u_k)\ \forall\ k \in \{0, 1, 2, ..., N-1\}$$
$$|\Delta u_k| \leq P_{\max}\ \forall\ k \in \{0, 1, 2, ..., N-1\}$$

where J is the cost function to be minimized, $P_{\max}$ is the limit on the inverter power, and Q and R, are the weighting matrices for control error penalty and control input penalty, respectively. The optimization solved over the time horizon length of N results in $\Delta u_k^* = \{\Delta u_0^*, \Delta u_1^*, ..., \Delta u_N^*\}$ with the first term of the sequence used as the control signal for the next sample as $\Delta u_k = \Delta u_0^*$.

B. MPC Base Case

MPC requires a model that predicts the microgrid frequency dynamics. Previously, in [13] a state space-based model developed according to Fig. 6 was used. In contrast, this paper uses a data-driven SI approach to provide the predictive model for MPC assuming no prior information on parameters and order of the system. However, a third-order model obtained through SI was selected for a fair comparison with an equivalent third-order model obtained from Fig. 6.

IV. System Modeling and Validation

The simulation setup for evaluating the data-driven MPC is shown in Fig. 7. The microgrid under study is a modified microgrid system from Cordova, Alaska [2]. The input and output of the frequency dynamics model are inverter power ΔP_{inv} and the change in microgrid frequency $\Delta\omega$ measured at the point-of-connection of the ESS. The input signal is a logarithmic chirp signal shown in Fig. 4. After the system is probed using an excitation signal, the output data are recorded. The SI process is an offline process where the data is used to estimate a transfer function model of the microgrid using SI instrumental variable estimation. Then, the obtained transfer function is changed into the state-space (SS) model. The frequency of the microgrid system is measured using a PLL. To emulate the real system noise, Gaussian noise with an SNR of 65 dB is added based on [2]. After obtaining the SI model, a KF-MPC control approach simulated in MATLAB/Simulink. The design parameters and design details of the MPC are based on [2], [13] and described in Section IV-B.

The normalized root-mean-square-error (NRMSE) calculates the fit of the model as:

$$NRMSE = 1 - \frac{||y - \hat{y}||}{||y - \text{mean}(y)||} \tag{3}$$

where, $y, \hat{y}$ are output data from the unidentified system, and output of the SI system respectively.

A. Linear Transformation of State Variables

The state variables that are obtained from the SS model are not directly related to the physical variables we know. For better intuition and model interpretability, the state variables need to be transformed into physical variables. One state variable we can choose is $\Delta\omega$ since we know it is the measurement. Since frequency supports require minimizing ROCOF,

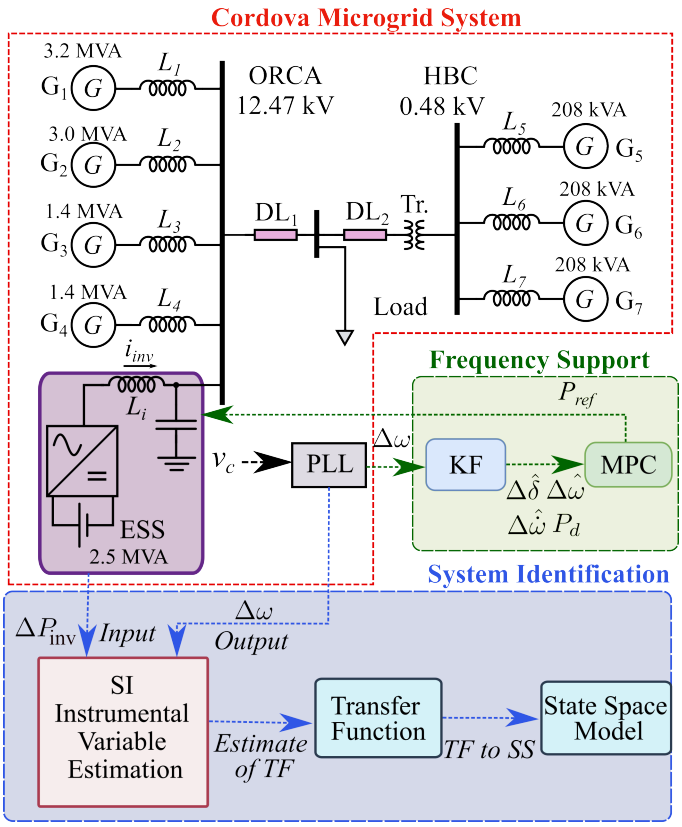

Fig. 7: Simulation setup for the system identification and KF-MPC frequency support where for SI input is the log square chirp signal P_{inv} to ESS and output is $\Delta\omega$ and for frequency support, KF estimates the states from the noisy measurement and MPC uses it to produce reference signal for ESS.

we can choose ROCOF ($\Delta\dot{\omega}$) as another state variable. We are free to choose a third-state variable. We have considered the integral of $\Delta\omega$ (power angle denoted by $\Delta\delta$) as another state. Then our final state vector is $\mathbf{x} = [\Delta\delta,\ \Delta\omega,\ \Delta\dot{\omega}]$. The linear transformation of any state variables can be computed as follows. Let the SS model of a system be:

$$\dot{\mathbf{x}} = \mathbf{A}\mathbf{x} + \mathbf{B}\mathbf{u}$$
$$\mathbf{y} = \mathbf{C}\mathbf{x} + \mathbf{D}\mathbf{u}$$

where **A, B, C**, and **D** are state space matrices, and **x, y**, and **u** are the states, output, and input of the system respectively. The system can be transformed into an alternate model having new matrices $\mathbf{A}_{new}, \mathbf{B}_{new}, \mathbf{C}_{new}, \mathbf{D}_{new}$ and new states **z** as:

$$\dot{\mathbf{z}} = \mathbf{A}_{new}\mathbf{z} + \mathbf{B}_{new}\mathbf{u}$$
$$\mathbf{y} = \mathbf{C}_{new}\mathbf{z} + \mathbf{D}_{new}\mathbf{u}$$

where $\mathbf{z} = \mathbf{T}\mathbf{x}, \mathbf{A}_{new} = \mathbf{T}\mathbf{A}\mathbf{T}^{-1}, \mathbf{B}_{new} = \mathbf{T}\mathbf{B}, \mathbf{C}_{new} = \mathbf{C}\mathbf{T}^{-1}, \mathbf{D}_{new} = \mathbf{D}$ and **T** is the transformation matrix.

B. KF-MPC Design Parameters

The MPC design parameters are sample time T_s, horizon length N, and weighting matrices for control error and control input Q and R. The eigenvalues obtained in section II-A gives the time constant of the system. The sample time is calculated based on the time constant and chosen to be approximately fifteen times smaller than the time constant [14] which is 0.02s. The horizon length is set for 50 samples (1s based on [2]. A horizon length should capture the performance of the frequency dynamics. On the other hand, a higher horizon length results in longer computational effort. Hence, horizon length should balance the computational cost and performance of the controller. For 50 samples, the horizon time is $1s$ for a $0.02s$ sample time. This value matches the time scale of the frequency dynamics of the system.

The matrix Q and R penalize poor system performance, and the control effect, respectively. In this paper, Q is a $diag(Q_{11}, Q_{22})$ where Q_{11} represents the weight for penalizing frequency deviation and Q_{22} is the weight for penalizing high ROCOF. Similarly, R penalizes the power output from the inverter. The values of Q_{11} and Q_{22} are 0.2 and 0.5 respectively based on [2]. This selection gives priority to minimizing ROCOF than the frequency deviation. Based on [2], the weight of R is 0.005.

For KF: a random 65 dB Gaussian measurement noise is added to the frequency based on [15]: measurement noise covariance ($R_{KF} = 10^{-7}$). The best weights are calculated using a parameter sweep. The objective of the parameter sweep was to obtain the estimation of the states as close to the PLL measurement data. The process noise covariance matrix for data-driven MPC system is $Q_{KF} = diag(300\times^{-9}, 2\times10^{-8}, 2.5\times10^{-8}, 200\times10^{-8})$. The matrix for the simplified transfer function model [13] is $Q_{KF} = diag(300\times^{-7}, 2\times10^{-9}, 2.5\times10^{-9}, 200\times10^{-7})$.

V. Results and Analysis

This section presents and analyzes SI training and testing result, the obtained state-space model, and MPC-KF frequency support result. The effect of the excitation signal on system harmonics is also presented.

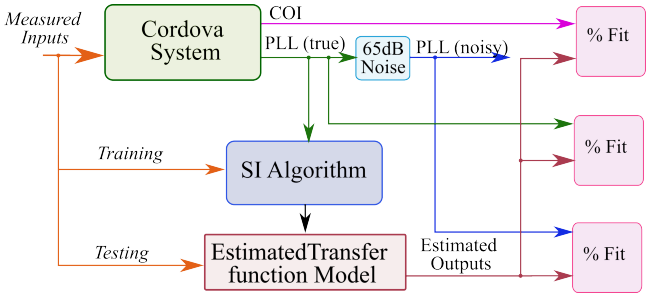

Fig. 8: The percent fit is calculated by comparing the actual outputs from the Cordova system: COI, PLL (true), PLL(noisy) with estimated outputs

In a power system, where different generators are present, the concept of Center of Inertia (COI) gives the correct estimation of the frequency. The COI can be calculated as:

$$COI = \frac{\sum_{i=1}^{N_g} \omega_i S_i}{\sum_{i=1}^{N_g} S_i} \tag{4}$$

where N_g is the total number of generators in the system, ω_i is the frequency measurement of i^{th} generator, and S_i is the apparent power of the i^{th} generator. Hence both COI and PLL data are used as a base for comparing the performance of SI.

Fig. 8 shows the process to compare the system identification result where the estimated transfer function result is compared with the COI, PLL true and noisy measurements.

A. System Identification Training and Test Result

TABLE II: % fit of Estimated TF having different poles and zeros with true PLL Data

Poles \ Zeroes	1	2	3
2	63.777	-	-
3	63.58	68.527	-
4	16.685	64.286	76.127

TABLE III: %fit of Estimated TF having different poles and zeros with true COI Data

Poles \ Zeroes	1	2	3
2	78.221	-	-
3	78.073	87.426	-
4	17.587	76.811	86.557

Tables II and III present the percentage fit of the training data (trained using PLL measurement only) with the true PLL and COI data for various poles and zeros. According to Table II, the best fit was achieved with four poles and three zeros. However, with the true COI data, the best fit was obtained with three poles and two zeros, as indicated in the Table III. Taking into account that the COI provides accurate measurements, a third-order model with three poles and two zeros is chosen as the best-fit model. Also, higher-order models involve more parameters and require more computational resources to solve the optimization problem at each sampling instant. This can result in longer computation time in MPC. The transfer function of the third order is shown in (5). Fig. 9 illustrates the comparison between the poles and zeros of the SI model and the model presented in [13].

$$G(s) = \frac{0.3727s^2 + 1.299s - 0.02979}{s^3 + 5.49s^2 + 30.50s + 2.364} \tag{5}$$

The training and testing results are compared to both the PLL and COI data. Fig. 11 presents the training and testing output waveform of PLL with noise, SI, PLL true, and COI data. The result indicates that utilization of noisy PLL measurements for training, the SI output exhibits frequency deviation close to true PLL and COI data.

In Fig. 10(a) percent fit of the training result is presented while Fig. 10(b) displays the percentage fit of the testing result for different frequency square wave signals. The result shows an improved fit to the COI, reflecting the noise in the PLL output values. As for the testing result, the fit percent is higher for low-frequency excitation signals. This is because PLL works better in a low-frequency range rather than a high one. The fit between the PLL data and COI data for larger frequencies is low.

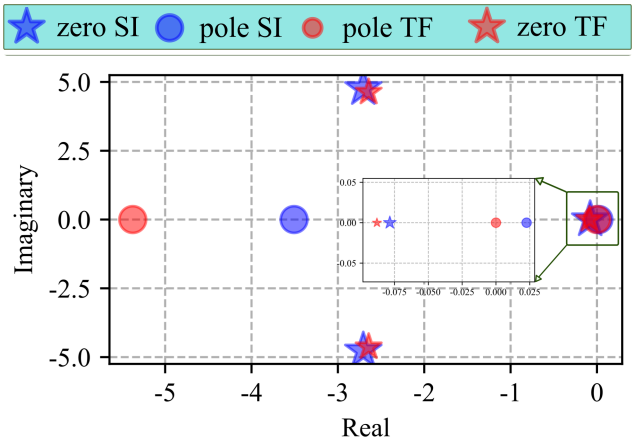

Fig. 9: Poles and zeroes of the SI model and model from [13]

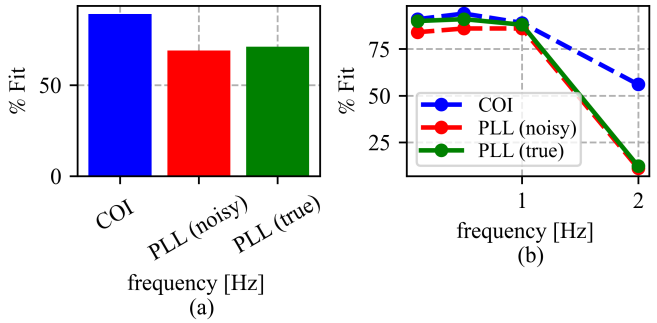

Fig. 10: Training and the testing result of SI (a) shows the training result using log chirp signal (b) shows the testing result for different frequency square wave

B. State Space Model

The SS model of the transfer function in (5) after transforming into state variables $[\Delta\delta \;\; \Delta\omega \;\; \Delta\dot{\omega}]^T$ are shown in (6). The transformation of the states is calculated as described in section IV-A.

$$A = \begin{bmatrix} 0 & 1 & 0 \\ 0 & 0 & 1 \\ -2.36 & -30.50 & -5.49 \end{bmatrix}; B = \begin{bmatrix} 0.0125 \\ 0.3727 \\ -0.7474 \end{bmatrix} \tag{6}$$

Now, introducing disturbance term P_d also as a state that represents the disturbance in the system. The term P_d is assumed as a parameter as it varies very slowly. P_d is augmented as a state because KF handles parameter estimation by augmenting parameters to states and setting its derivative to zero [16]. Therefore, the KF estimates the disturbance term as well. The disturbance of the system can be predicted for a system as long as the dimension of disturbance is less than or equal to the measurement [17]. Hence, the new states variables are $[\Delta\delta \;\; \Delta\omega \;\; \Delta\dot{\omega} \;\; P_d]^T$ for estimation.

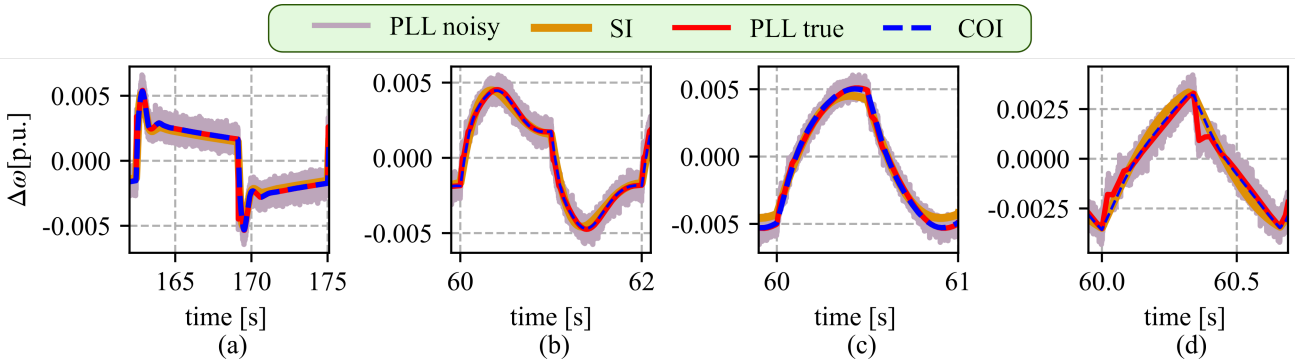

Fig. 11: Training and testing output waveform (a) show the training result (b-d) shows the testing results for 0.5, 1, and 1.5Hz respectively.

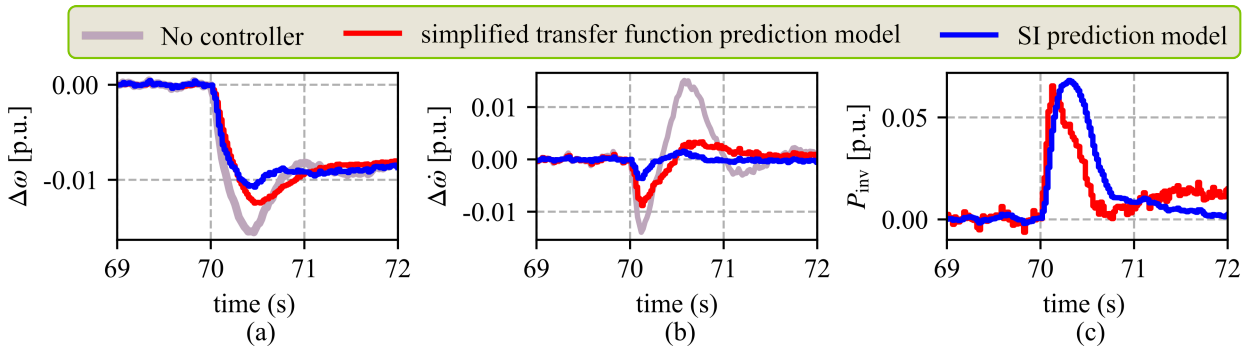

Fig. 12: (a) Frequency, (b) ROCOF, and (c) peak-power output of ESS for a step-change load in MATLAB/Simulink using simplified TF prediction model [13] and SI prediction model.

$$A = \begin{bmatrix} 0 & 1 & 0 & 0 \\ 0 & 0 & 1 & 0 \\ & & & \\ -2.36 & -30.50 & -5.49 & 1 \\ 0 & 0 & 0 & 0 \end{bmatrix}; B = \begin{bmatrix} 0.0125 \\ 0.3727 \\ -0.7474 \\ 0 \end{bmatrix} \tag{7}$$

C. MPC Frequency Support Result

Fig. 12 shows a comparison of different models for frequency support. It shows that the two predictive models of MPC: simplified transfer function model [13] and SI predictive model we derived using SI, provide fast-frequency support. The frequency support provided by these models is better than when there is no MPC. The comparison of the simplified transfer function model with the SI predictive model shows SI predictive model has less frequency and ROCOF deviation. However, if we observe the inverter power in Fig. 12(c), the SI-based MPC predictive model uses more inverter power than the simplified TF-based MPC. Although the power curve is different as shown in fig. 12(c): the peak power difference between the two is insignificant. Thus, the model obtained using SI utilizes a slightly higher amount of inverter power to reduce the frequency deviation.

D. MPC Computation Time

Fig. 13 presents a box plot comparing the computation time of two prediction models used in MPC. The results

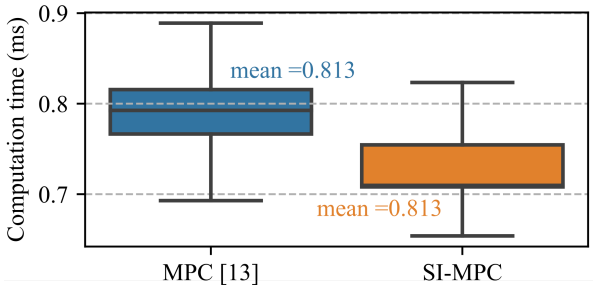

Fig. 13: Box plot showing the computation time of MPC using simplified TF prediction model [13] and SI prediction model.

indicate that the mean computation time of MPC using the SI prediction model is approximately 3.30% lower than that of MPC with a simplified SS model [13]. While this reduction in computation time is not significant, it can be attributed to the SI predictive model utilizing a state space matrix with pre-determined numerical values. In contrast, the model in [13] calculates each element of the state-space matrix based on values represented in the transfer function model.

E. Effects of Chirp Signal on System Harmonics

The total harmonics distortion (THD) calculates the ratio of the root mean square (RMS) of the harmonic content, which includes harmonic components up to the 50^{th} order while excluding interharmonics, expressed as a percentage of the fundamental frequency [18]. According to IEEE standard

519 [18], the assessment of very short-time harmonics involves evaluating their values over a 3-second timeframe. The Fourier coefficients of 12-cycle windows are calculated for a 60 Hz power system. Then, the Fourier coefficients of each individual frequency component are aggregated based on the RMS calculation, and the THD from aggregated Fourier coefficients is calculated. This analysis aims to understand and quantify the harmonic content present during this short duration. The sampling frequency in our case is 1 MHz and the switching frequency is 20 kHz.

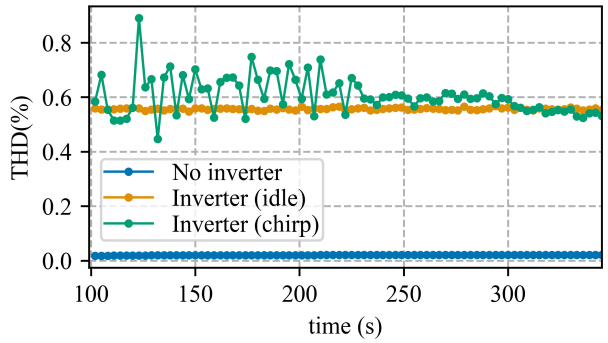

Fig. 14: very short THD of the system for every 3 seconds without an inverter, with an idle inverter, and with chirp signal injected to the inverter.

Fig. 14 illustrates the THD of the system under investigation, in the absence of an inverter, when the inverter is idle (chirp signal is not injected into the system), and when the chirp signal is injected into the system. In accordance with the guidelines presented in the IEEE Standard 519 [18], it is recommended that the THD of the source voltage remains below 5%. The results demonstrate that the THD values for the system meet the prescribed threshold under all three conditions: when the inverter is idle, when the system is excited with the square chirp signal, and when the inverter is absent from the system.

VI. Conclusion

The paper implements system identification in MATLAB/Simulink to predict the model of a microgrid. The model was validated on testing data and the goodness of fit showed the third-order model best fitted the data. The model was used as a predictive model for MPC and was compared with the third-order simplified model. The result showed that the model utilizes the control action to produce a better result than the previous model. Also, the harmonics analysis showed that the THD with a square chirp signal is within the IEEE standard limit. In the future, we aim to conduct and compare the harmonics analysis for different ordered SI prediction models. The SI process, as it currently stands, is conducted offline. However, there is potential for future development where the SI process could be performed online. This would involve collecting data in real time and estimating the model at a slower time scale. The resulting model could then be used as a predictive model within the framework of MPC for effective frequency control.

VII. Acknowledgements

The authors thank Dr. Hyungjin Choi for the technical review of this paper.

References

[1] N. Bhujel, A. Rai, T. M. Hansen, R. Tonkoski, and U. Tamrakar, "A model predictive approach for voltage support in microgrids using energy storage systems," in *2021 IEEE Power & Energy Society General Meeting (PESGM)*, 2021, pp. 1–5.

[2] U. Tamrakar, D. A. Copp, T. Nguyen, T. M. Hansen, and R. Tonkoski, "Optimization-based fast-frequency estimation and control of low-inertia microgrids," *IEEE Transactions on Energy Conversion*, vol. 36, no. 2, pp. 1459–1468, 2021.

[3] Z. Yan and Y. Xu, "Data-driven load frequency control for stochastic power systems: A deep reinforcement learning method with continuous action search," *IEEE Transactions on Power Systems*, vol. 34, no. 2, pp. 1653–1656, 2019.

[4] H. A. Yousef, K. AL-Kharusi, M. H. Albadi, and N. Hosseinzadeh, "Load frequency control of a multi-area power system: An adaptive fuzzy logic approach," *IEEE Transactions on Power Systems*, vol. 29, no. 4, pp. 1822–1830, 2014.

[5] D. J. Ryan, R. Razzaghi, H. D. Torresan, A. Karimi, and B. Bahrani, "Grid-supporting battery energy storage systems in islanded microgrids: A data-driven control approach," *IEEE Transactions on Sustainable Energy*, vol. 12, no. 2, pp. 834–846, 2021.

[6] W. Liu, G. Geng, Q. Jiang, H. Fan, and J. Yu, "Model-free fast frequency control support with energy storage system," *IEEE Transactions on Power Systems*, vol. 35, no. 4, pp. 3078–3086, 2020.

[7] L. Ljung, *System identification: Theory for the user*. Prentice Hall PTR, 2012.

[8] R. Chakraborty, H. Jain, and G.-S. Seo, "A review of active probing-based system identification techniques with applications in power systems," *International Journal of Electrical Power & Energy Systems*, vol. 140, p. 108008, 2022.

[9] N. Guruwacharya, N. Bhujel, U. Tamrakar, M. Rauniyar, S. Subedi, S. E. Berg, T. M. Hansen, and R. Tonkoski, "Data-driven power electronic converter modeling for low inertia power system dynamic studies," in *2020 IEEE Power & Energy Society General Meeting (PESGM)*, 2020, pp. 1–5.

[10] T. Tay, I. Mareels, and J. Moore, *High Performance Control*, ser. Progress in Mathematics. Birkhäuser, 1998.

[11] P. Burrascano, S. Laureti, L. Senni, G. Silipigni, R. Tomasello, and M. Ricci, "Chirp design in a pulse compression procedure for the identification of non-linear systems," in *2017 14th International Conference on Synthesis, Modeling, Analysis and Simulation Methods and Applications to Circuit Design (SMACD)*, 2017, pp. 1–4.

[12] B. Poudel, P. Aslami, T. Aryal, N. Bhujel, A. Rai, M. Rauniyar, H. M. Rekabdarkolaee, U. Tamrakar, T. M. Hansen, and R. Tonkoski, "Comparative analysis of state and parameter estimation techniques for power system frequency dynamics," in *2022 International Symposium on Power Electronics, Electrical Drives, Automation and Motion (SPEEDAM)*, 2022, pp. 754–761.

[13] A. Rai, N. Bhujel, T. M. Hansen, R. Tonkoski, and U. Tamrakar, "Implementation of model predictive control for frequency support in a real-time digital simulator," in *2022 IEEE Electrical Energy Storage Application and Technologies Conference (EESAT)*, 2022, pp. 1–5.

[14] N. Bhujel, T. M. Hansen, R. Tonkoski, U. Tamrakar, and R. H. Byrne, "Model predictive integrated voltage and frequency support in microgrids," in 52^{nd} *North American Power Symposium (NAPS)*, 2021, pp. 1–6.

[15] U. Tamrakar, D. A. Copp, T. A. Nguyen, T. M. Hansen, and R. Tonkoski, "Real-time estimation of microgrid inertia and damping constant," *IEEE Access*, vol. 9, pp. 114 523–114 534, 2021.

[16] D. Simon, *Optimal State Estimation: Kalman, H Infinity, and Nonlinear Approaches*. Wiley, 2006. [Online]. Available: https://books.google.com/books?id=UiMVoP_7TZkC

[17] J. B. Rawlings, D. Q. Mayne, and M. Diehl, *Model predictive control: Theory, computation, and design*. Nob Hill Publishing, 2020.

[18] "IEEE standard for harmonic control in electric power systems," *IEEE Std 519-2022 (Revision of IEEE Std 519-2014)*, pp. 1–31, 2022.